Decoupled Control of Flexure Jointed Hexapods Using Estimated Joint Space Mass-Inertia Matrix

Yixin Chen and John E. McInroy

Yixin Chen is with the Department of Computer Science and Engineering, The Pennsylvania State University, University Park, PA 16801, USA. Research was performed when the author was with the Department of Electrical Engineering, University of Wyoming. E-mail:yixchen@cse.psu.edu.

John E. McInroy is with the Department of Electrical Engineering, University of Wyoming, WY, 82071 USA. E-mail:mcinroy@uwyo.edu.

Abstract

By exploiting properties of the joint space mass-inertia matrix of flexure jointed hexapods (or Stewart platforms), a new decoupling method is proposed. The new decoupling method, through a static input-output mapping, transforms the highly coupled 6 input 6 output dynamics into 6 independent single-input single-output (SISO) channels. Controls for these SISO channels are far simpler than their multiple-input multiple-output (MIMO) counterparts. Prior decoupling control methods imposed severe constraints on the allowable geometry and payload. The new method loosens and removes these constraints, thus greatly expanding the applications. Based on the new decoupling method, identification algorithms using the Constrained Least Squares (CLS) and the Symmetric Positive Definite Estimation (SPDE) methods are introduced to estimate the joint space mass-inertia matrix using payload accelerations and base forces. These identification algorithms can be used for precision payload calibration, thus improving performance and removing the labor required to design the control for different payloads. The new decoupling method, together with the identification algorithms, is experimentally compared to earlier techniques. These experimental results indicate that the new approach is practical and improves performance.

Keywords

Vibration isolation, decoupling control, Stewart platform, precision robots, hexapod, symmetric positive definite matrix, identification.

I. Introduction

Several researchers have developed flexure jointed hexapods for micro-precision applications in which only a very small workspace is required ([20],[19],[1],[5],[6],[18],[15],[16]). A hexapod, which is also sometimes called a Stewart platform, consists of six legs connecting a payload to a base via spherical joints (Figure 1). To avoid the extremely nonlinear micro-dynamics of joint friction and backlash, flexure jointed hexapods employ flexure joints. A flexure joint bends material to achieve motion, rather than sliding or rolling across two surfaces. This does eliminate friction and backlash, but adds spring dynamics and limits the workspace. Compared to non-flexure jointed hexapods, flexure jointed hexapods have several distinct characteristics [13]:

- The flexures greatly alter the dynamic behavior.
- The base motion is a significant contributor to the overall motion, even when the base is subjected only to ambient seismic vibrations.
- Because the workspace is so small, linearized dynamic models are highly accurate.

McInroy [11] developed and validated the dynamics of a flexure jointed hexapod. Using this model, [13] proposed two decoupling algorithms by combining static input-output transformations with hexapod geometric design.

These decoupling algorithms impose three major constraints [13]:

- All six struts must have same mass, damping, and stiffness.
- The payload mass-inertia matrix, found with respect to the base frame, must be diagonal.
- The geometry of the hexapod and the attachment of the payload to the hexapod must be carefully chosen.

The first constraint requires that all six struts of a hexapod be physically identical. The second constraint requires that the base frame be selected to coincide with the orientation of the principal axes of the payload. The third constraint depends on the hexapod's geometry. For instance, if a mutually orthogonal geometry has been selected [14], the payload's center of mass must coincide with the center of the cube formed by the orthogonal struts ([18] provides more geometric details).

Although these constraints are possible to be satisfied for some specific applications, they limit the applications significantly. For instance, in order to satisfy the second and the third constraints, the payload on the University of Wyoming (UW) hexapod requires a complicated, custom designed truss structure. Any changes to the payload requires a new truss structure, so minor changes are prohibitively expensive. Moreover, the last constraint seriously limits the location of the end effector, thus eliminating a lot of important applications such as those requiring cooperating hexapods. The algorithm derived herein relaxes the first constraint and removes the highly restrictive second and third constraints, thus greatly expanding the potential applications. For instance, by removing the geometry constraints, geometries matched to particular needs can be used. Similarly, new payloads can easily be accommodated.

Unlike the work by Ghorbel *et al.* [7], which proposes a set point PD control with guaranteed stability under the domain of validity of the model for a broad class of robots including Stewart platforms, the techniques presented here is a static decoupling approach applicable to the much smaller class of flexure jointed hexapods. Although the idea of decoupling MIMO plants into SISO plants is not new, most plants cannot be statically de-

coupled, while the class of flexure jointed hexapods can be. This is because the workspace is very small, thus the Jacobian matrix (relating payload Cartesian movements to strut length changes in the joint space) and the rotation matrix from the payload frame to the base frame can be viewed as constant matrices, the Coriolis and centripetal terms can be neglected [13], [12]. Static decoupling approach facilitates advanced control features such as adaptation, fault tolerance, iterative learning, etc. Consequently, they offer improved performance for a number of applications including motion simulation [17], precision pointing ([19], [15]), and vibration isolation ([20], [1], [6], [18]).

To further improve performance and ease of use, two identification algorithms, based on the CLS (Constrained Least Squares) and the SPDE (Symmetric Positive Definite Estimation), are proposed to estimate the joint space mass-inertia matrix from payload accelerations and base forces. This allows new payloads to be quickly incorporated without the labor and potential errors that accompany model based approaches. Furthermore, it allows precision calibration of the dynamics to increase the performance over that attained when using modeled, vs. measured parameters. Experimental results on the UW hexapod indicate that the decoupling and identification algorithms are practical, and yield superior performance.

The remainder of the paper is organized as follows. Section II reviews one model for flexure jointed hexapods. Section III presents the main theoretical contributions of the paper: static input-output decoupling transformations that convert the multiple-input, multiple-output dynamics into single-input, single-output form. Section IV eases the implementation of the new decoupling technique by developing new methods for accurately measuring the required mass/inertia matrix. Finally, Section V presents experimental results on the University of Wyoming hexapod.

II. Dynamic Model of Flexure Jointed Hexapods

This section briefly summarizes the dynamic model of flexure jointed hexapods. See [2], [11] for details. Figure 1 illustrates a general flexure jointed hexapod. Like any hexapod, it consists of a base, a payload, and six struts that can change their lengths. The struts, which have spherical joints at both ends, connect the payload to the base.

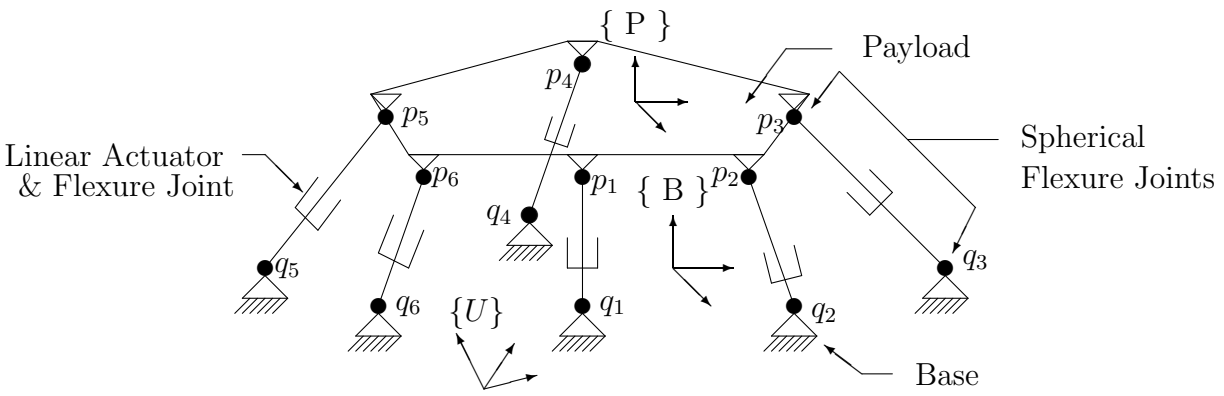

Fig. 1. A flexure jointed hexapod (or Stewart Platform). $\{P\}$ is a Cartesian coordinate frame located at, and rigidly attached to, the payload's center of mass. $\{B\}$ is the frame attached to the (possibly moving) base, and $\{U\}$ is a Universal inertial frame of reference.

The simplified dynamics of a flexure jointed hexapod are written as [2]

$$\vec{f_b} = \vec{f_m} - \mathbf{K}(\vec{p}_s - \vec{q}_s - \vec{l}_r) - \mathbf{B}(\dot{\vec{p}}_s - \dot{\vec{q}}_s) \quad (1)$$

$$\mathbf{M}_p\ddot{\vec{p}}_s + \mathbf{B}\dot{\vec{p}}_s + \mathbf{K}\vec{p}_s = \vec{f_m} + \mathbf{M}_q\ddot{\vec{q}}_s + \mathbf{B}\dot{\vec{q}}_s + \mathbf{K}\vec{q}_s + \mathbf{J}^{-T}{}_B^U\mathbf{R}^T\vec{\mathcal{F}}_e \quad (2)$$

where

$$\mathbf{M}_p = \mathbf{J}^{-T}{}_P^B\mathbf{R}^P\mathbf{M}_x{}_P^B\mathbf{R}^T\mathbf{J}^{-1} + \mathbf{M}_s$$

$$\mathbf{M}_q = \mathbf{J}^{-T}{}_P^B\mathbf{R}^P\mathbf{M}_x{}_P^B\mathbf{R}^T\mathbf{J}^{-1} - \mathbf{J}^{-T}{}_P^B\mathbf{R}^P\mathbf{M}_x{}_P^U\mathbf{R}^T\mathbf{J}_c{\mathbf{J}_B}^{-1}$$

are joint space mass-inertia matrices. Here

- $\mathbf{J}$ is the 6×6 hexapod Jacobian relating payload Cartesian movements, expressed in the $\{B\}$ frame, to strut length changes in the joint space;
- ${}_B^U\mathbf{R}$ is the 6×6 rotation matrix from the base frame, $\{B\}$, to the Universal inertial frame of reference $\{U\}$ (it consists of two identical 3×3 rotation matrices forming a block diagonal 6×6 matrix). Similarly, ${}_P^B\mathbf{R}$ is the rotation matrix from the payload frame to the base frame, and ${}_P^U\mathbf{R} = {}_B^U\mathbf{R}\,{}_P^B\mathbf{R}$;
- $\mathbf{J}_c$ and $\mathbf{J}_B$ are 6×6 Jacobian matrices capturing base motion;
- ${}^P\mathbf{M}_x$ is the 6×6 mass-inertia matrix of the payload, found with respect to the payload frame, $\{P\}$, whose origin is at the hexapod payload's center of mass;

- $\mathbf{M}_s$ is a diagonal 6×6 matrix containing the moving mass of each strut;
- $\mathbf{B}$ and $\mathbf{K}$ are 6×6 diagonal matrices containing the damping and stiffness, respectively, of each strut;
- $\vec{l_r}$ is the constant 6×1 vector of relaxed strut lengths;
- $\vec{f_b}$ is the 6×1 vector of forces exerted at the bottom of the strut;
- $\vec{f_m}$ is the 6×1 vector of strut motor forces;
- $\vec{p}_s = [\vec{v}_1^T \vec{p}_1, ..., \vec{v}_6^T \vec{p}_6]^T$ and $\vec{q}_s = [\vec{v}_1^T \vec{q}_1, ..., \vec{v}_6^T \vec{q}_6]^T$ are 6×1 vectors where $\vec{p}_i$ denotes the three dimensional attachment point of the i^{th} strut to the payload, $\vec{q}_i$ denotes the attachment point of the i^{th} strut to the base, and $\vec{v}_i$ is the unit direction vector of the i^{th} strut pointing from $\vec{q}_i$ to $\vec{p}_i$ ($\vec{p}_i$, $\vec{q}_i$, and $\vec{v}_i$ are expressed in the same coordinate frame). Consequently, $\vec{p}_s - \vec{q}_s$ is the 6×1 vector of strut lengths;
- $\vec{\mathcal{F}}_e$ is a 6×1 vector of payload exogenous generalized forces applied at the origin of the $\{P\}$ frame.

Since the struts can only move very small distances, the Jacobian matrices ($\mathbf{J}$, $\mathbf{J}_c$, and $\mathbf{J}_B$) and the rotation matrix (${}^B_P\mathbf{R}$) are all nearly constant [13]. The algorithms developed in this paper assume that $\mathbf{J}$ and ${}^B_P\mathbf{R}$ are constant. This does, of course, limit the applications somewhat, but is in practice highly accurate because the flexure joints severely limit the workspace anyway. Several industrial applications (including precision manipulation, vibration isolation, and motion simulation) already exist, and the results of this paper apply to all of these fields. Recently, McInroy [12] provides experimental verification of the above dynamics model and gives design criteria to make sure that model is good (by designing the mechanical system to fit the model).

III. Decoupling the Dynamics of Flexure Jointed Hexapods

This section first discusses three constraints imposed by the prior decoupling algorithms [13]. Then, it introduces a new decoupling method that relaxes the first constraint and removes the remaining constraints.

A. Constraints of the Prior Decoupling Methods

McInroy and Hamann [13] proposed two decoupling algorithms, using $\mathbf{J}^T$ or $\mathbf{J}^{-1}$ as decoupling transformations, which can be used in the "quiet box" problem (using payload

acceleration, velocity, or position measurements to control the payload motion) and the "dirty box" problem (using base force feedback to minimize the transmission of forces to the base). However three conditions must be met in order to make the algorithms apply [13]:

- The strut mass, damping, and stiffness matrices are scaled identities, $\mathbf{M}_s = m\mathbf{I}$, $\mathbf{B} = b\mathbf{I}$, $\mathbf{K} = k\mathbf{I}$.
- The payload mass-inertia matrix (${}^B\mathbf{M}_x$) found with respect to the base frame $\{B\}$ is diagonal.
- $\mathbf{J}^T\mathbf{J}$ is diagonal over the whole workspace.

The first condition is easily satisfied whenever the struts are identical in construction (they may differ in length) which is true and desirable for many applications. But there are some applications that require different strut properties. For instance, in some hexapods, three struts contributing to the translating movements are identical, and the remaining three contributing to the rotating movements are also identical. But the strut properties are different between the two groups. In this case, $\mathbf{M}_s$, $\mathbf{B}$, and $\mathbf{K}$ are only diagonal.

The second condition is slightly more restrictive. The payload mass-inertia matrix (${}^B\mathbf{M}_x$), found with respect to the base frame $\{B\}$, consists of two blocks, one expressing mass and the other expressing inertial properties of the payload,

$$\begin{aligned} {}^B\mathbf{M}_x &= {}^B_P\mathbf{R}\,{}^P\mathbf{M}_x\,{}^B_P\mathbf{R}^T \\ &= \begin{bmatrix} m_p\mathbf{I}_{3\times3} & \mathbf{0}_{3\times3} \\ \mathbf{0}_{3\times3} & {}^B_P\mathbf{R}\,{}^c\mathbf{I}\,{}^B_P\mathbf{R}^T \end{bmatrix} \end{aligned} \tag{3}$$

where m_p is the payload mass, and ${}^c\mathbf{I}$ is the inertia tensor [4] of the payload with respect to the payload frame $\{P\}$. The upper block, $m_p\mathbf{I}_{3\times3}$, is always diagonal. The lower block, ${}^B_P\mathbf{R}\,{}^c\mathbf{I}\,{}^B_P\mathbf{R}^T$, can be diagonal if there exists three orthogonal axes of symmetry with the payload mass distributed symmetrically about these axes. It is then diagonal if $\{B\}$ is selected to have the same orientation as these axes. This condition can be satisfied as long as the payload is a fixed rigid body. In this paper, the payload is supposed to be a fixed rigid body. This assumption is made partly to simplify the approach and partly because all known flexure jointed hexapods satisfy this constraint. Thus this condition can usually be satisfied, although finding the principal axes of a payload is laborious, especially when

the payload changes often.

The last condition is by far the most restrictive. It relies heavily on the hexapod geometric design. Three hexapod configurations satisfying the geometry requirements are proposed in [13]. In all of these configurations, the payload's center of mass must be placed in some position determined by the corresponding hexapod geometry since the Jacobian, $\mathbf{J}$, is a function of the payload's center of mass. Thus any changes to the payload require at least the tedious procedure of computing and adjusting the position of the payload's center of mass by adding or reducing some counterweights. Furthermore, this constraint significantly limits the location of the end effector, thus eliminating many important applications. For example, the close quarters required for dual hexapods performing micro-manipulation tasks prohibit the mass balancing required by earlier methods.

B. Decoupling the Dynamics using Simultaneous Diagonalization

The new decoupling algorithm is based on the simultaneous diagonalization of $\mathbf{M}_p$, $\mathbf{B}$, and $\mathbf{K}$ matrices. Instead of being scaled identities, $\mathbf{M}_s$, $\mathbf{B}$ and $\mathbf{K}$ are only required to be diagonal matrices satisfying $\mathbf{B} = \alpha\mathbf{K}$, where α is a nonzero scalar constant. In addition, the remaining much more restrictive conditions are removed. The algorithm is suitable for both the "quiet box" and "dirty box" problems.

B.1 Simultaneous Diagonalization by Similarity

First, consider the case where $\mathbf{B}$ and $\mathbf{K}$ are scaled identities ($\mathbf{B}$ not necessarily equals $\mathbf{K}$). This happens when all six struts of the hexapod are identical in damping and stiffness, while they may be different in mass and length.

From (3), it is easily seen that ${}^{B}\mathbf{M}_x$ is symmetric. This implies that

$$\begin{aligned} \mathbf{M}_p{}^T &= (\mathbf{J}^{-1})^T {}^{B}\mathbf{M}_x{}^T (\mathbf{J}^{-T})^T + \mathbf{M}_s{}^T \\ &= \mathbf{J}^{-T\,B}\mathbf{M}_x\mathbf{J}^{-1} + \mathbf{M}_s \\ &= \mathbf{M}_p \ . \end{aligned} \tag{4}$$

Hence the joint space mass-inertia matrix $\mathbf{M}_p$ is symmetric. Thus it can be unitarily diagonalized using the Schur Decomposition (Theorem 7.1.3, [8])

$$\mathbf{M}_p = \mathbf{V}\mathbf{D}\mathbf{V}^T \tag{5}$$

where $\mathbf{V}$ is an orthogonal matrix ($\mathbf{V}\mathbf{V}^T = \mathbf{V}^T\mathbf{V} = \mathbf{I}$), and $\mathbf{D}$ is a diagonal matrix.

$\mathbf{B}$ and $\mathbf{K}$ are obviously diagonalizable by similarity. Since they are scaled identities, they also commute with each other and $\mathbf{M}_p$ under multiplication. Thus from the fact that a set of diagonalizable (by similarity) matrices are simultaneously diagonalizable if and only if each pair in the set commutes under multiplication (Theorem 1.3.19, [10]), $\{\mathbf{M}_p, \mathbf{B}, \mathbf{K}\}$ is simultaneously diagonalizable. Moreover, $\mathbf{V}$ in (5) is an orthogonal diagonalization transformation, such that $\mathbf{V}^T\mathbf{M}_p\mathbf{V} = \mathbf{D}$, $\mathbf{V}^T\mathbf{B}\mathbf{V} = \mathbf{B}$, $\mathbf{V}^T\mathbf{K}\mathbf{V} = \mathbf{K}$.

For the "quiet box" problem, the dynamic model is described by equation (2). Define a new input and a new output by

$$\begin{aligned} \vec{u} &= \mathbf{V}^T\vec{f}_m \\ \vec{y} &= \mathbf{V}^T\vec{p}_s\,. \end{aligned}$$

Then (2) can be written as

$$\mathbf{D}\ddot{\vec{y}} + \mathbf{B}\dot{\vec{y}} + \mathbf{K}\vec{y} = \vec{u} + \mathbf{V}^T(\mathbf{M}_q\ddot{\vec{q}}_s + \mathbf{B}\dot{\vec{q}}_s + \mathbf{K}\vec{q}_s) + \mathbf{V}^T\mathbf{J}^{-T}{}^U_B\mathbf{R}^T\vec{\mathcal{F}}_e\,. \tag{6}$$

Note that $\mathbf{D}$, $\mathbf{B}$, and $\mathbf{K}$ matrices are diagonal. Consequently, the dynamics from $\vec{u}$ to $\vec{y}$ are LTI (Linear Time Invariant) decoupled, and independent SISO controls can be designed. In addition to simplifying nominal control design, this also facilitates fault tolerant controls [15]. Based on (6), SISO LTI control algorithms can be designed to suppress the base movement ($\ddot{\vec{q}}_s$, $\dot{\vec{q}}_s$, and $\vec{q}_s$) and exogenous force ($\vec{\mathcal{F}}_e$) influences on the payload.

For "dirty box" vibration isolation applications, base forces are typically fed back, rather than payload positions, velocities or accelerations. Assuming the base is stationary or can only move over small ranges, i.e., $\mathbf{M}_q$ and ${}^U_B\mathbf{R}$ in (2) can be regarded as constant matrices. The algorithm may be re-formulated to cover "dirty box" problems as follows. First, substituting (1) into (2), assuming $\vec{l}_r$ and $\vec{\mathcal{G}}$ terms cancel each other (because of small base movements), and solving for $\vec{f}_b$ gives

$$\vec{f}_b = \mathbf{M}_p\ddot{\vec{p}}_s - \mathbf{M}_q\ddot{\vec{q}}_s - \mathbf{J}^{-T}{}^U_B\mathbf{R}^T\vec{\mathcal{F}}_e\ . \tag{7}$$

Since $\mathbf{M}_q$ and ${}^U_B\mathbf{R}$ are constant, equations (2) and (7) are LTI. Thus Laplace transforms

can be taken to yield

$$\vec{f}_b = \mathbf{M}_p s^2 \vec{p}_s - \mathbf{M}_q s^2 \vec{q}_s - \mathbf{J}^{-T}{}_B^U \mathbf{R}^T \vec{\mathcal{F}}_e \tag{8}$$

$$(\mathbf{M}_p s^2 + \mathbf{B}s + \mathbf{K})\vec{p}_s = \vec{f}_m + (\mathbf{M}_q s^2 + \mathbf{B}s + \mathbf{K})\vec{q}_s + \mathbf{J}^{-T}{}_B^U \mathbf{R}^T \vec{\mathcal{F}}_e \,. \tag{9}$$

Then inserting (8) into (9) and rearranging terms yields

$$\begin{aligned} \vec{f}_b = {} & \mathbf{M}_p s^2 (\mathbf{M}_p s^2 + \mathbf{B}s + \mathbf{K})^{-1} \vec{f}_m - \mathbf{M}_q s^2 \vec{q}_s + \\ & \mathbf{M}_p s^2 (\mathbf{M}_p s^2 + \mathbf{B}s + \mathbf{K})^{-1} (\mathbf{M}_q s^2 + \mathbf{B}s + \mathbf{K}) \vec{q}_s + \\ & [\mathbf{M}_p s^2 (\mathbf{M}_p s^2 + \mathbf{B}s + \mathbf{K})^{-1} - \mathbf{I}] \mathbf{J}^{-T}{}_B^U \mathbf{R}^T \vec{\mathcal{F}}_e \ . \end{aligned} \tag{10}$$

Define a new input and a new output

$$\vec{u} = \mathbf{V}^T \vec{f}_m \tag{11}$$

$$\vec{y} = \mathbf{V}^T \vec{f}_b \tag{12}$$

where $\mathbf{V}$ is defined by (5). Then (10) becomes

$$\begin{aligned} \vec{y} = {} & \mathbf{D}s^2 (\mathbf{D}s^2 + \mathbf{B}s + \mathbf{K})^{-1} \vec{u} - \mathbf{V}^T \mathbf{M}_q s^2 \vec{q}_s + \\ & \mathbf{D}s^2 (\mathbf{D}s^2 + \mathbf{B}s + \mathbf{K})^{-1} \mathbf{V}^T (\mathbf{M}_q s^2 + \mathbf{B}s + \mathbf{K}) \vec{q}_s + \\ & [\mathbf{D}s^2 (\mathbf{D}s^2 + \mathbf{B}s + \mathbf{K})^{-1} - \mathbf{I}] \mathbf{V}^T \mathbf{J}^{-T}{}_B^U \mathbf{R}^T \vec{\mathcal{F}}_e \ . \end{aligned}$$

Since $\mathbf{D}s^2(\mathbf{D}s^2 + \mathbf{B}s + \mathbf{K})^{-1}$ is a diagonal transfer function matrix, once again, the dynamics from $\vec{u}$ to $\vec{y}$ are decoupled. SISO LTI compensators from $\vec{u}$ to $\vec{y}$ can be designed to suppress the base acceleration and exogenous force disturbances. Note that this can be viewed in two ways. If $\vec{\mathcal{F}}_e$ is the dominant disturbance, then the control provides dirty box isolation. If $\vec{q}_s$ is the dominant disturbance, then the hexapod attempts to quiet a vibrating structure.

B.2 Simultaneous Diagonalization by Congruence

In some applications, the struts have different physical properties, i.e., $\mathbf{M}_s$, $\mathbf{B}$, and $\mathbf{K}$ matrices are only diagonal (not necessarily identities). Thus the algorithms in section III-B.1 are no longer valid. However, if the $\mathbf{B}$ and $\mathbf{K}$ satisfy the condition $\mathbf{B} = \alpha\mathbf{K}$ where α is a nonzero scalar constant, then $\mathbf{M}_p$, $\mathbf{B}$, and $\mathbf{K}$ matrices can still be simultaneously diagonalized.

Equation (4) shows that $\mathbf{M}_p$ is symmetric. In fact, $\mathbf{M}_p$ is also positive definite. This fact comes from the intrinsic physical property of $\mathbf{M}_p$ matrix. The kinetic energy of the payload is defined by

$$K_e = \frac{1}{2}\dot{\chi}^T \mathbf{M}_p \dot{\chi}$$

where K_e is the kinetic energy of the payload, $\dot{\chi}$ is the payload's generalized , or spatial velocity. Since $K_e > 0$ for all $\dot{\chi} \neq \vec{0}$, it can be concluded that $\mathbf{M}_p$ is positive definite.

Since $\mathbf{M}_p$ is positive definite and $\mathbf{B}$ is symmetric, there exists a nonsingular matrix $\mathbf{C}$ such that $\mathbf{C}^T\mathbf{M}_p\mathbf{C}$ and $\mathbf{C}^T\mathbf{B}\mathbf{C}$ are both diagonal (Theorem 7.6.6, [10]). Moreover, $\mathbf{C}$ can be calculated as follows. First, calculate the Schur decomposition of $\mathbf{M}_p$, which is given by (5). Since $\mathbf{M}_p$ is positive definite, all the diagonal entries of $\mathbf{D}$ are positive. Next, define a new matrix by

$$\mathbf{B}_1 = \mathbf{D}^{-\frac{1}{2}}\mathbf{V}^T\mathbf{B}\mathbf{V}\mathbf{D}^{-\frac{1}{2}}.$$

It is obvious that $\mathbf{B}_1$ is symmetric, thus the Schur decomposition is given by

$$\mathbf{B}_1 = \mathbf{U}\mathbf{\Lambda}\mathbf{U}^T$$

where $\mathbf{U}$ is an orthogonal matrix and $\mathbf{\Lambda}$ is a diagonal matrix. Finally, the simultaneous diagonalization matrix, which is invertible, is given by

$$\mathbf{C} = \mathbf{V}\mathbf{D}^{-\frac{1}{2}}\mathbf{U} \ .$$

It can be easily shown that $\mathbf{C}^T\mathbf{M}_p\mathbf{C} = \mathbf{I}$ and $\mathbf{C}^T\mathbf{B}\mathbf{C} = \mathbf{\Lambda}$. Furthermore, if $\mathbf{B} = \alpha\mathbf{K}$, then $\mathbf{C}^T\mathbf{K}\mathbf{C} = \frac{1}{\alpha}\mathbf{\Lambda}$. Thus, $\mathbf{C}$ simultaneously diagonalizes $\mathbf{M}_p$, $\mathbf{B}$, and $\mathbf{K}$ matrices.

For the "quiet box" problem, a new input and a new output are defined by

$$\begin{aligned} \vec{u} &= \mathbf{C}^T\vec{f}_m \\ \vec{y} &= \mathbf{C}^{-1}\vec{p}_s \, . \end{aligned}$$

Then (2) can be written as

$$\ddot{\vec{y}} + \mathbf{\Lambda}\dot{\vec{y}} + \frac{1}{\alpha}\mathbf{\Lambda}\vec{y} = \vec{u} + \mathbf{C}^T\mathbf{J}^{-T}{}^U_B\mathbf{R}^T\vec{\mathcal{F}}_e + \mathbf{C}^T(\mathbf{M}_q\ddot{\vec{q}}_s + \mathbf{B}\dot{\vec{q}}_s + \mathbf{K}\vec{q}_s) \, . \tag{13}$$

The dynamics from $\vec{u}$ to $\vec{y}$ are LTI decoupled. Based on (13), SISO LTI control algorithms can be designed to suppress the base movement ($\ddot{\vec{q}}_s$, $\dot{\vec{q}}_s$, and $\vec{q}_s$) and exogenous force ($\vec{\mathcal{F}}_e$) influences on the payload.

Similarly, for the "dirty box" problem, a new input and a new output are defined by

$$\begin{aligned} \vec{u} &= \mathbf{C}^T \vec{f}_m \\ \vec{y} &= \mathbf{C}^T \vec{f}_b \, . \end{aligned}$$

Then (10) can be written as

$$\begin{aligned} \vec{y} = s^2(\mathbf{I}s^2 + \mathbf{\Lambda}s + \frac{1}{\alpha}\mathbf{\Lambda})^{-1}\vec{u} - \mathbf{C}^T\mathbf{M}_q s^2 \vec{q}_s + \\ s^2(\mathbf{I}s^2 + \alpha s + \tfrac{1}{\alpha}\mathbf{\Lambda})^{-1}\mathbf{C}^T(\mathbf{M}_q s^2 + \mathbf{B}s + \mathbf{K})\vec{q}_s + \\ [s^2(\mathbf{I}s^2 + \mathbf{\Lambda}s + \tfrac{1}{\alpha}\mathbf{\Lambda})^{-1} - \mathbf{I}]\mathbf{C}^T\mathbf{J}^{-T}{}^U_B\mathbf{R}^T\vec{\mathcal{F}}_e \ . \end{aligned}$$

Since $s^2(\mathbf{I}s^2 + \mathbf{\Lambda}s + \frac{1}{\alpha}\mathbf{\Lambda})^{-1}$ is a diagonal transfer function matrix, once again, the dynamics from $\vec{u}$ to $\vec{y}$ are decoupled. SISO LTI compensators from $\vec{u}$ to $\vec{y}$ can be designed to suppress the base acceleration and exogenous force disturbances.

IV. Identification of Joint Space Mass-Inertia Matrix

Section III-B proposes two transformation matrices ($\mathbf{V}$ and $\mathbf{C}$) which can decouple the dynamic model of a flexure jointed hexapod. In order to calculate $\mathbf{V}$ or $\mathbf{C}$, $\mathbf{M}_p$ must be known. There are two ways of obtaining $\mathbf{M}_p$. One way is to calculate $\mathbf{M}_p$ from the design parameters of the hexapod. The other is to identify $\mathbf{M}_p$ from measurements. The former method requires exact values of $\mathbf{M}_s$, ${}^P\mathbf{M}_x$, ${}^B_P\mathbf{R}$, and $\mathbf{J}$, which in practice is laborious to calculate and can introduce errors. This section summarizes two algorithms of directly identifying $\mathbf{M}_p$ so performance can be retained despite manufacturing variances, payload changes, etc.

If the base is kept stationary and there are no exogenous generalized forces exerted on the payload when doing the identification experiment (these constraints can be easily satisfied) then $\ddot{\vec{q}}_s = \vec{0}$ and $\vec{\mathcal{F}}_e = \vec{0}$. Thus (7) becomes

$$\vec{f}_b = \mathbf{M}_p \ddot{\vec{p}}_s \ . \tag{14}$$

The accelerometers can only measure the acceleration along the strut directions, $\ddot{\vec{p}}_u$, defined by

$$\ddot{\vec{p}}_u = \left[\vec{v}_1^T\ddot{\vec{p}}_1, \ \ldots, \ \vec{v}_6^T\ddot{\vec{p}}_6\right]^T .$$

Since the vectors $\vec{v}_i$ are unit vectors along the i^{th} strut direction, $\dot{\vec{v}}_i^T \vec{v}_i = 0$. This also implies that $\dot{\vec{v}}_i^T(\vec{p}_i - \vec{q}_i) = 0$ and $\ddot{\vec{v}}_i^T(\vec{p}_i - \vec{q}_i) + \dot{\vec{v}}_i^T(\dot{\vec{p}}_i - \dot{\vec{q}}_i) = 0$. The difference between $\ddot{\vec{p}}_s - \ddot{\vec{q}}_s$ and $\ddot{\vec{p}}_u$ is then found to be

$$\ddot{\vec{p}}_s - \ddot{\vec{q}}_s = \ddot{\vec{p}}_u + \vec{\mathcal{C}} - \left[\dot{\vec{v}}_1^T \dot{\vec{q}}_1, \ldots, \dot{\vec{v}}_6^T \dot{\vec{q}}_6\right]^T - \left[\vec{v}_1^T \ddot{\vec{q}}_1, \ldots, \vec{v}_6^T \ddot{\vec{q}}_6\right]^T$$

where $\vec{\mathcal{C}} = \left[\dot{\vec{v}}_1^T \dot{\vec{p}}_1, \ldots, \dot{\vec{v}}_6^T \dot{\vec{p}}_6\right]^T$ is a vector of Coriolis terms. As shown in the Appendix, the energy of $\vec{\mathcal{C}}_1$ is negligible with respect to that of $\ddot{\vec{p}}_u$ when the passband of the activation signal is chosen judiciously. If the base is held stationary during identification experiments, then $\dot{\vec{q}}_i = \ddot{\vec{q}}_i = \ddot{\vec{q}}_s = 0$. Thus (14) can be approximately written as

$$\vec{f}_b = \mathbf{M}_p \ddot{\vec{p}}_u \ . \tag{15}$$

This implies that if both the base forces ($\vec{f}_b$) and accelerations along the strut direction ($\ddot{\vec{p}}_u$) are measured, then $\mathbf{M}_p$ can be estimated. The main subtlety is that $\mathbf{M}_p$ is symmetric and positive definite.

Now the identification problem is to find a matrix solution $\hat{\mathbf{M}}_p$ for equations

$$\hat{\vec{f}}_b^k = \hat{\mathbf{M}}_p \hat{\ddot{\vec{p}}}_u^k, \ k = 1, ..., N$$

with the constraints $\hat{\mathbf{M}}_p$ being symmetric and positive definite. N is the number of the samples, $\hat{\vec{f}}_b^k$ is the measured vector of base forces at time k, and $\hat{\ddot{\vec{p}}}_u^k$ is the measured vector of payload attachment point acceleration along struts at time k.

By combining the N equations together, (15) can be written as

$$\mathbf{F} = \hat{\mathbf{M}}_p \mathbf{P}$$

where

$$\begin{aligned} \mathbf{F} &= \left[\hat{\vec{f}}_b^1, \hat{\vec{f}}_b^2, \ldots, \hat{\vec{f}}_b^N\right] \\ \mathbf{P} &= \left[\hat{\ddot{\vec{p}}}_u^1, \hat{\ddot{\vec{p}}}_u^2, \ldots, \hat{\ddot{\vec{p}}}_u^N\right] \ . \end{aligned}$$

This constrained estimation problem can be solved in many ways. Next, two algorithms based on different optimization criteria are summarized.

The first algorithm is called the Symmetric Procrustes (SP) method [9]. It seeks to minimize the least squares criterion $\|\hat{\mathbf{M}}_p\mathbf{P}-\mathbf{F}\|_F^2$ for all symmetric $\hat{\mathbf{M}}_p$, where $\|.\|_F$ denotes the Frobenius (or Euclidean) norm. Higham [9] shows that the global optimizers are the solutions of the Lyapunov equation

$$\mathbf{P}\mathbf{P}^T\mathbf{X} + \mathbf{X}\mathbf{P}\mathbf{P}^T = \mathbf{P}\mathbf{F}^T + \mathbf{F}\mathbf{P}^T$$

where $\mathbf{X}$ is the unknown matrix. If the rows of $\mathbf{P}$ are linearly independent, then the global minimizer is unique. However, the definiteness of the solution depends on the definiteness of $\mathbf{P}\mathbf{F}^T + \mathbf{F}\mathbf{P}^T$. If $\mathbf{P}\mathbf{F}^T + \mathbf{F}\mathbf{P}^T$ is positive (semi-)definite, then the global minimizer is positive (semi-)definite. If $\mathbf{P}\mathbf{F}^T + \mathbf{F}\mathbf{P}^T$ is indefinite, we can not conclude anything about the definiteness of the global minimizer. Thus the SP method can only handle the symmetric constraint.

The second algorithm is called the Symmetric Positive Definite Estimation (SPDE) method [3] that employs both the symmetric and the positive definite constraints. The criterion it seeks to minimize is $\|\mathbf{Y}\mathbf{P} - \mathbf{Y}^{-T}\mathbf{F}\|_F^2$ for all invertible $\mathbf{Y}$ with $\mathbf{Y}^T\mathbf{Y} = \hat{\mathbf{M}}_p$. If the rows of $\mathbf{P}$ are linearly independent, then the unique global minimizer is given by

$$\hat{\mathbf{M}}_p = \mathbf{U}\boldsymbol{\Sigma}_\mathbf{1}^{-\mathbf{1}}\mathbf{V}\boldsymbol{\Sigma}_\mathbf{2}\mathbf{V}^T\boldsymbol{\Sigma}_\mathbf{1}^{-\mathbf{1}}\mathbf{U}^T \tag{16}$$

where

$$\begin{aligned}
\mathbf{U}\boldsymbol{\Sigma}_\mathbf{1}\mathbf{U}^T\mathbf{U}\boldsymbol{\Sigma}_\mathbf{1}\mathbf{U}^T &= \mathbf{P}\mathbf{P}^T \\
\mathbf{U}^T\mathbf{U} &= \mathbf{I} \\
\boldsymbol{\Sigma}_\mathbf{1} &= \mathrm{diag}[\sqrt{\lambda_1}, \ldots, \sqrt{\lambda_6}] \\
\mathbf{V}\boldsymbol{\Sigma}_\mathbf{2}\mathbf{V}^T\mathbf{V}\boldsymbol{\Sigma}_\mathbf{2}\mathbf{V}^T &= \boldsymbol{\Sigma}_\mathbf{1}\mathbf{U}^T\mathbf{F}\mathbf{F}^T\mathbf{U}\boldsymbol{\Sigma}_\mathbf{1} \\
\mathbf{V}^T\mathbf{V} &= \mathbf{I} \\
\boldsymbol{\Sigma}_\mathbf{2} &= \mathrm{diag}[\sqrt{\sigma_1}, \ldots, \sqrt{\sigma_6}]
\end{aligned}$$

$\lambda_1, \ldots, \lambda_6$ are eigenvalues of $\mathbf{P}\mathbf{P}^T$, and $\sigma_1, \ldots, \sigma_6$ are eigenvalues of $\boldsymbol{\Sigma}_\mathbf{1}\mathbf{U}^T\mathbf{F}\mathbf{F}^T\mathbf{U}\boldsymbol{\Sigma}_\mathbf{1}$. Note that as long as $\mathbf{P}$ is of full rank, the optimal estimate $\hat{\mathbf{M}}_p$ is always symmetric and positive definite.

Compared with the SPDE method, the SP method, in general, gives a better estimate if the sampling and instrument errors are solely confined to $\mathbf{F}$, and, of course, if $\mathbf{P}\mathbf{F}^T+\mathbf{F}\mathbf{P}^T$ is

positive definite. However, if errors also appear in $\mathbf{P}$, which is exactly what happened in our case since both $\mathbf{F}$ and $\mathbf{P}$ contain the measurements accompanied by noises (or errors), the SPDE method generates a better estimate [3]. This is because the optimization criterion of the SPDE method takes the errors in both $\mathbf{F}$ and $\mathbf{P}$ into consideration. Moreover, the symmetric and positive definite constraint is naturally embedded into the criterion. Consequently, the SPDE method is used in the experiments described in the next section.

V. Experimental Results

The identification and decoupling algorithms have been experimentally verified on one of the UW's mutually orthogonal hexapods. The mechanical parts of the hexapod are all custom machined based on a NASA Jet Propulsion Laboratory design. All six struts are identical. A 200 MHz Gateway 2000 Pentium II computer running the QNX real time operating system sends commands through Computers Boards 16 bit DAC converters to Techron linear current amplifiers. These power BEI voice coil actuators, resulting in base forces ($\vec{f}_b$) measured by PCB quartz force rings mounted on the bottom end of each strut, and payload accelerations along the strut direction ($\ddot{\vec{p}}_u$) measured by KISTLER-BEAM accelerometers mounted on the top of the spherical joint connecting the payload. The force and acceleration signals are sampled by the control computer's 16 bit analog to digital converters at a rate of 5kHz. Each strut has a maximum stroke of $\pm$ .025 inches.

For the identification experiment, six independent random-noise signals pass through six digital low-pass filters with cutoff frequencies at 80Hz (this value is based on the analysis provided in the Appendix). Then the filtered signals are sent to all six voice coil actuators to generate vibrations. 256K samples (each sample includes 6 base forces and 6 payload accelerations) are collected. Based on (16), the estimated joint space mass-inertia matrix $\hat{\mathbf{M}}_p$ is calculated.

The performance of the new algorithm will be compared to that obtained using the algorithm in [13]. In [13], a new input and a new output are defined as

$$\vec{u} = \mathbf{J}^T \vec{f}_m \tag{17}$$

$$\vec{y} = \mathbf{J}^T \vec{f}_b \tag{18}$$

Bode magnitude plots from u_5 (input of channel 5) to $\vec{y}$ (all six channels) are shown in

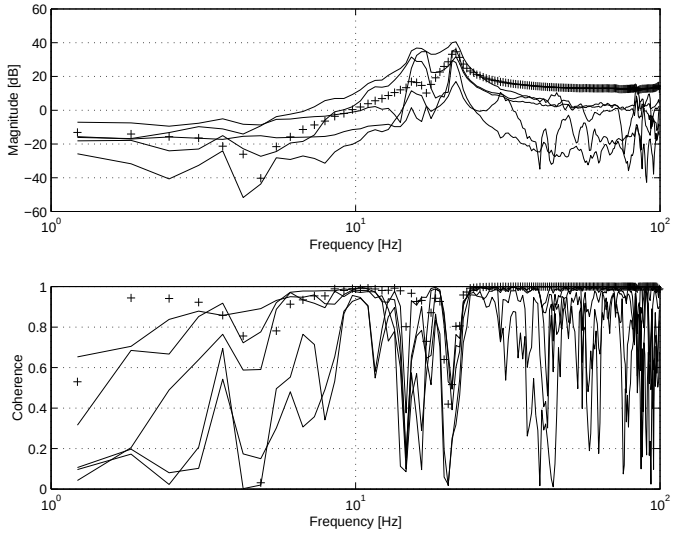

Fig. 2. Bode magnitude plot and coherence from u_5 (input of channel 5) to $\vec{y}$. y_5 (output of channel 5) is denoted by "+" signs. $\mathbf{J}^T$ is decoupling matrix. The payload's center of mass does not coincide with the center of the cube formed by six orthogonal struts.

Figure 2.

Using the $\mathbf{M}_p$ matrix calculated from the design parameters of the hexapod, a new input and a new output are defined using (11) and (12). Bode magnitude plots from u_5 to $\vec{y}$ are shown in Figure 3.

Finally using the results of the identification experiment, $\hat{\mathbf{M}}_p$, a new input and a new output are found from (11) and (12). Bode magnitude plots from u_5 to $\vec{y}$ are shown in Figure 4.

In the experiments, the counterweight placed on the payload is removed. Thus the payload's center of mass doesn't coincide with the center of the cube formed by the orthogonal struts. This explains the results in Figure 2. We can see that using decoupling transformations (17) and (18), there are still strong couplings among all six channels. The input channel (channel 5) is difficult to distinguish from the others. However, using the calculated $\mathbf{M_p}$ matrix and the new decoupling transform (11) and (12), channel 5 is 3 times (10 dB) stronger in the frequency range 30Hz to 100Hz (Figure 3). When the estimated joint space mass-inertia matrix $\hat{\mathbf{M}}_p$ and the new decoupling transform (11) and (12) are used, channel 5 is almost 10 times (20dB) stronger across nearly all frequencies (in Figure 4). In addition, in all three experiments, the transfer function estimate for channel 5 displays

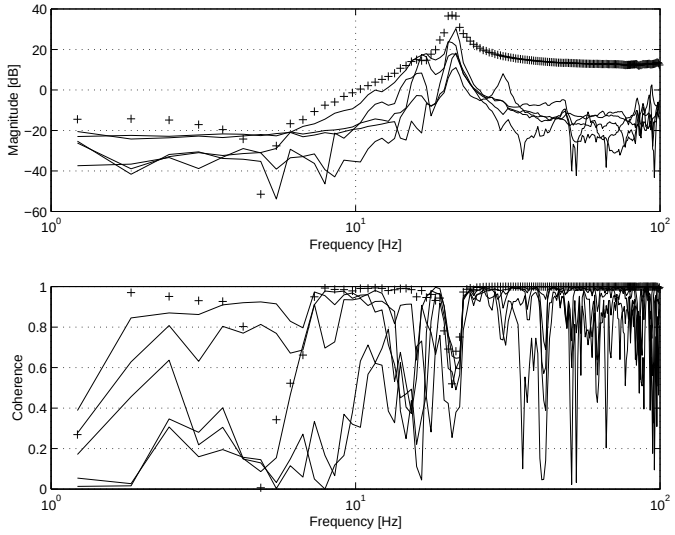

Fig. 3. Bode magnitude plot and coherence from u_5 (input of channel 5) to $\vec{y}$. y_5 (output of channel 5) is denoted by "+" signs. $\mathbf{V}^T$ is decoupling matrix ($\mathbf{V}^T$ is calculated from $\mathbf{M}_p$). The payload's center of mass does not coincide with the center of the cube formed by six orthogonal struts.

much more coherence than the other channels. Moreover, among the transfer function estimates for channel 5, the estimated transfer function using the identified decoupling matrix shows the best coherence.

VI. Conclusions

Compared to the earlier decoupling methods [13], the new algorithm puts far less constraints on the geometric and payload design of a hexapod:

- All six struts need not be physically identical, i.e., $\mathbf{M}_s$, $\mathbf{B}$, and $\mathbf{K}$ are only required to be diagonal matrices satisfying $\mathbf{B} = \alpha\mathbf{K}$ where α is a nonzero scalar constant.
- The base frame $\{B\}$ can be chosen arbitrarily, i.e., the payload mass-inertia matrix ${}^B\mathbf{M}_x$ found with respect to the base frame need not be a diagonal matrix.
- $\mathbf{J}^T\mathbf{J}$ need not be a diagonal matrix. Thus geometries matched to particular needs can be used, and new payloads can be easily accommodated.

In general, the new decoupling algorithm greatly expands the potential applications.

In order to get the new decoupling matrix $\mathbf{V}$ or $\mathbf{C}$, $\mathbf{M}_p$ must be known. While $\mathbf{M}_p$ can be calculated by system parameters, the process is cumbersome when the payload changes often, and is sensitive to modeling errors. Consequently, two algorithms (SP and SPDE)

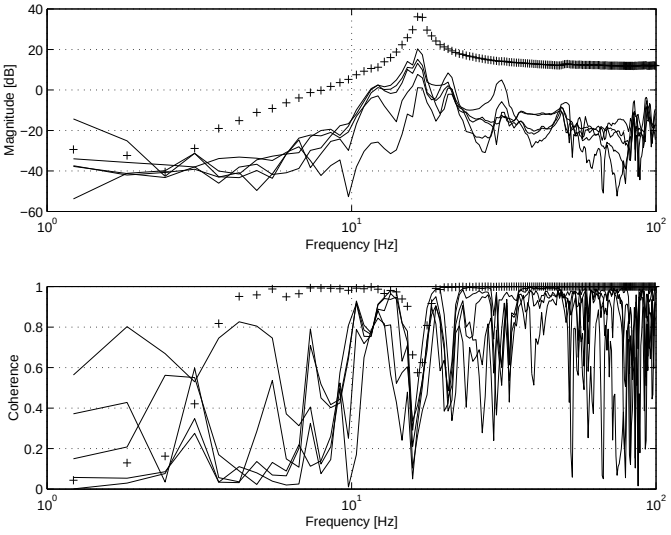

Fig. 4. Bode magnitude plot and coherence from u_5 (input of channel 5) to $\vec{y}$. y_5 (output of channel 5) is denoted by "+" signs. $\mathbf{V}^T$ is decoupling matrix ($\mathbf{V}^T$ is calculated from $\hat{\mathbf{M}}_p$). The payload's center of mass does not coincide with the center of the cube formed by six orthogonal struts.

for identification of $\mathbf{M}_p$ are summarized. Both algorithms use the measured base force and payload acceleration along the strut direction to estimate $\mathbf{M}_p$. The SP method can only handle the symmetric constraint. While the SPDE method employs both the symmetric and the positive definite constraints, and it also gives a better estimate if noises appear in both $\mathbf{F}$ and $\mathbf{P}$.

Experimental results verify that the new approaches are practical, and yield good performance.

Acknowledgments

This work was supported by the Ballistic Missile Defense Organization and Army Research Office under grants DAAG55-98-1-0007 and DAAD19-00-1-0153. The authors would like to thank anonymous reviewers and the associate editor for their comments that led to improvements in this paper.

References

[1] E.H. Anderson, D.J. Leo, and M.D. Holcomb, Ultraquiet Platform for Active Vibration Isolation, in *Proc. of the SPIE Smart Structure and Materials Conf.*, pp. 436-451, 1996.

[2] Y. Chen and J.E. McInroy, Identification and decoupling control of flexure jointed hexapods, in *Proc. IEEE Int. Conf. Robotics and Automation*. San Francisco, CA USA, pp. 1936–1941, April 2000.

[3] Y. Chen and J.E. McInroy, Estimation of Symmetric, Positive Definite Matrices from Imperfect Measurements, *IEEE Trans. on Automatic Control*, 2002 (to appear).

[4] J.J. Craig, *Introduction to Robotics: Mechanics and Control*, Reading, MA: Addison-Wesley, 1986.

[5] Z.J. Geng and L.S. Haynes, Six Degree-of-Freedom Active Vibration Control Using the Stewart Platforms, *IEEE Trans. on Control Systems Technology*, vol. 2, pp. 45-53, March 1994.

[6] Z.J. Geng, G.G. Pan, L.S. Haynes, B.K. Wada, and J.A. Garba, An Intelligent Control System for Multiple Degree-of-Freedom Vibration Isolation, *Journal of Intelligent Material Systems and Structures*, vol. 6, pp. 787-800, November 1995.

[7] F. Ghorbel, O. Chetelat, R. Gunawardana, and R. Longchamp, Modeling and Set Point Control of Closed-Chain Mechanisms: Theory and Experiment, *IEEE Trans. on Control Systems Technology*, Vol. 8, pp. 801-815, Sept. 2000.

[8] G.H. Golub and C.F. Van Loan, *Matrix Computation, 3rd ed.*, Johns Hopkins University Press, Baltimore, MD, 1996.

[9] N.J. Higham, The Symmetric Procrustes Problem, *BIT*, 28, pp. 133-143, 1988.

[10] R.A. Horn and C.R. Johnson, *Matrix Analysis,* Cambridge University Press, 1990.

[11] J.E. McInroy, Dynamic Modeling of Flexure Jointed Hexapods for Control Purposes, in *Proc. IEEE Conf. on Control Applications*, Kona, Hawaii, pp. 508-513, August 1999.

[12] J.E. McInroy, Modeling and Design of Flexure Jointed Stewart Platforms for Control Purposes, *Accepted IEEE/ASME Transactions on Mechatronics*, 2002.

[13] J.E. McInroy and J.C. Hamann, Design and Control of Flexure Jointed Hexapods, *IEEE Trans. on Robotics and Automation*, Vol. 16, pp. 372-381, August 2000.

[14] J.E. McInroy, J.F. O'Brien, and G. Neat, Method and Experimental Validation of a Precision, Reconfigurable Pointing Control Strategy, in *Proc. IEEE Conf. on Decision and Control*, San Diego, CA, December 1997.

[15] J.E. McInroy, J.F. O'Brien, and G.W. Neat, Precise, Fault Tolerant Pointing Using a Stewart Platform, *IEEE/ASME Trans. on Mechatronics*, vol. 4, pp. 91-95, March 1999.

[16] J.F. O'Brien, J.E. McInroy, D. Bodtke, M. Bruch, and J.C. Hamann, Lessons Learned in Nonlinear Systems and Flexible Robots Through Experiments on a 6 Legged Platform, in *Proc. American Control Conf.*, vol 3, Philadelphia, PA, pp. 868-872, 1998.

[17] R. Peterson and J.C. Hobson, High Frequency Motion Simulator, *SPIE Conference*, April, 2001.

[18] J. Spanos, Z. Rahman, and G. Blackwood, A Soft 6-axis Active Vibration Isolator, in *Proc. of the American Control Conf.*, pp. 412-416, 1995.

[19] J. Sullivan, A. Rahman, R. Cobb, and J. Spanos, Closed-Loop Performance of a Vibration Isolation and Suppression System, in *Proc. of the American Control Conf.*, pp. 3974-3978, 1997.

[20] D. Thayer, J. Vagners, A. Von Flotow, C. Hardham, and K. Scribner, Six-Axis Vibration Isolation Systems Using Soft Actuators and Multiple Sensors, in *Proc. of the Annual American Astronautical Society (AAS) Rocky Mountain Guidance and Control Conf.*, pp. 497-506, 1998.

Appendix

Here we provide a justification of the claim in Section IV: $\ddot{\vec{p}}_s \approx \ddot{\vec{p}}_u$ in the sense that $\vec{\mathcal{C}} = [\dot{\vec{v}}_1^T \vec{p}_1, \ldots, \dot{\vec{v}}_6^T \vec{p}_6]^T$ is negligible in terms of energy. Due to the symmetric and mutually orthogonal geometry [13] of the UW's flexure jointed hexapod, it suffices to consider two struts as plotted in Figure 5.

Let $\vec{p}(t) = \vec{p}_1(t) = \vec{p}_2(t)$ be the position of attachment points of struts 1 and 2 to the payload at time

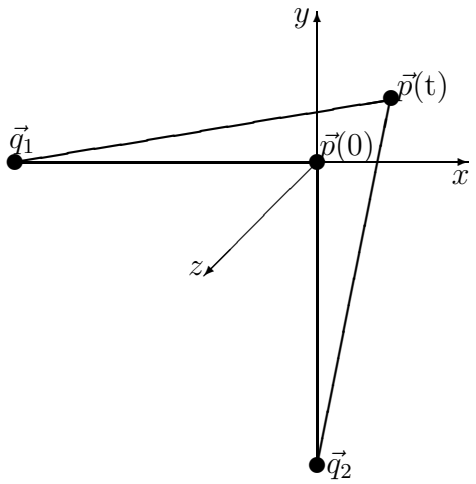

Fig. 5. Two struts of a flexure jointed hexapod.

t ($\vec{p}(0)$ being the nominal position). Let $\vec{q}_1$ and $\vec{q}_2$ be stationary attachment points of struts 1 and 2 to the base, respectively. All struts have identical relaxed lengths L and maximum stroke of $\pm S$. For UW's flexure jointed hexapod, $L = 16$ inches and $S = 0.025$ inches, thus $S \ll L$. Let the trajectory of payload attachment point be $\vec{p}(t) = [Ax(t), Ay(t), Az(t)]^T$ where $A = \frac{S}{2}$, $x(t)$, $y(t)$, and $z(t)$ are band-limited white noises distributed on $(-1, 1)$ with variance σ^2 and passband $[-W, W]$.

The unit vector $\vec{v}_1$ pointing from $\vec{q}_1$ to $\vec{p}_1$ is

$$\vec{v}_1 = \frac{1}{\sqrt{(Ax(t)+L)^2 + A^2y(t)^2 + A^2z(t)^2}} \begin{bmatrix} Ax(t)+L \\ Ay(t) \\ Az(t) \end{bmatrix}$$

Since $A \ll L$, $\vec{v}_1$ can be approximately written as

$$\vec{v}_1 \approx \frac{1}{L} \begin{bmatrix} L \\ Ay(t) \\ Az(t) \end{bmatrix} \quad . \tag{19}$$

Based on (19), we have

$$\begin{aligned} \vec{v}_1^T \ddot{\vec{p}}_1 &= A\ddot{x} + \frac{A^2}{L}(\ddot{y}y + \ddot{z}z) \\ \dot{\vec{v}}_1^T \dot{\vec{p}}_1 &= \frac{A^2}{L}(\dot{y}^2 + \dot{z}^2) \end{aligned}$$

Let $X(j\omega)$, $Y(j\omega)$, and $Z(j\omega)$ be the Fourier transforms of $x(t)$, $y(t)$, and $z(t)$, respectively. Then

$$|X(j\omega)| = |Y(j\omega)| = |Z(j\omega)| = \begin{cases} \sigma & |\omega| \le W \\ 0 & |\omega| > W \end{cases} \quad .$$

From the differentiation properties, the Fourier transforms of $\dot{x}$, $\dot{y}$, $\dot{z}$, $\ddot{x}$, $\ddot{y}$, and $\ddot{z}$ are $j\omega X(j\omega)$, $j\omega Y(j\omega)$, $j\omega Z(j\omega)$, $-\omega^2 X(j\omega)$, $-\omega^2 Y(j\omega)$, and $-\omega^2 Z(j\omega)$, respectively. Then, an upperbound on $|\dot{x}(t)|$ can be derived as

$$|\dot{x}(t)| = \frac{1}{2\pi}\left|\int_{-\infty}^{+\infty} j\omega X(j\omega)e^{j\omega t}d\omega\right| \leq \frac{1}{2\pi}\int_{-\infty}^{+\infty}\left|j\omega X(j\omega)e^{j\omega t}\right|d\omega = \frac{1}{2\pi}\int_{-W}^{+W}\sigma|\omega|d\omega = \frac{\sigma W^2}{2\pi} \quad . \quad (20)$$

Similarly, we have $|\dot{y}(t)| \leq \frac{\sigma W^2}{2\pi}$ and $|\dot{z}(t)| \leq \frac{\sigma W^2}{2\pi}$. From the Parseval's relation, we have

$$\int_{-\infty}^{+\infty}\ddot{x}^2 dt = \frac{1}{2\pi}\int_{-\infty}^{+\infty}\left|-\omega^2 X(j\omega)\right|^2 d\omega = \frac{1}{2\pi}\int_{-W}^{+W}\sigma^2\omega^4 d\omega = \frac{\sigma^2 W^5}{5\pi} \quad ,$$

and

$$\int_{-\infty}^{+\infty}\dot{x}^2 dt = \frac{1}{2\pi}\int_{-\infty}^{+\infty}\left|j\omega X(j\omega)\right|^2 d\omega = \frac{1}{2\pi}\int_{-W}^{+W}\sigma^2\omega^2 d\omega = \frac{\sigma^2 W^3}{3\pi} \quad .$$

Similar derivations show that $\int_{-\infty}^{+\infty}\ddot{y}^2 dt = \int_{-\infty}^{+\infty}\ddot{z}^2 dt = \frac{\sigma^2 W^5}{5\pi}$ and $\int_{-\infty}^{+\infty}\dot{y}^2 dt = \int_{-\infty}^{+\infty}\dot{z}^2 dt = \frac{\sigma^2 W^3}{3\pi}$.

Now, a lower bound for the energy of $\vec{v}_1^T\ddot{\vec{p}}_1$, which is defined by $E_1 = \int_{-\infty}^{+\infty}(\vec{v}_1^T\ddot{\vec{p}}_1)^2 dt$, is built as follows

$$\begin{aligned}
E_1 &= \int_{-\infty}^{+\infty}\left[A\ddot{x} + \frac{A^2}{L}(\ddot{y}y + \ddot{z}z)\right]^2 dt \quad \geq \quad \int_{-\infty}^{+\infty}\left[A^2\ddot{x}^2 - \frac{2A^3}{L}\left|\ddot{x}(\ddot{y}y + \ddot{z}z)\right|\right]dt \\
&\geq A^2\int_{-\infty}^{+\infty}\ddot{x}^2 dt - \frac{2A^3}{L}\sqrt{\int_{-\infty}^{+\infty}\ddot{x}^2 dt\int_{-\infty}^{+\infty}(\ddot{y}y + \ddot{z}z)^2 dt} \quad (21) \\
&\geq A^2\int_{-\infty}^{+\infty}\ddot{x}^2 dt - \frac{2A^3}{L}\sqrt{\int_{-\infty}^{+\infty}\ddot{x}^2 dt}\left(\sqrt{\int_{-\infty}^{+\infty}\ddot{y}^2 y^2 dt} + \sqrt{\int_{-\infty}^{+\infty}\ddot{z}^2 z^2 dt}\right) \quad (22) \\
&\geq A^2\int_{-\infty}^{+\infty}\ddot{x}^2 dt - \frac{2A^3}{L}\sqrt{\int_{-\infty}^{+\infty}\ddot{x}^2 dt}\left(\sqrt{\int_{-\infty}^{+\infty}\ddot{y}^2 dt} + \sqrt{\int_{-\infty}^{+\infty}\ddot{z}^2 dt}\right) \quad (23) \\
&= A^2\frac{\sigma^2 W^5}{5\pi} - \frac{2A^3}{L}\sqrt{\frac{\sigma^2 W^5}{5\pi}}\left(\sqrt{\frac{\sigma^2 W^5}{5\pi}} + \sqrt{\frac{\sigma^2 W^5}{5\pi}}\right) \\
&= \left(1 - \frac{4A}{L}\right)\frac{A^2\sigma^2 W^5}{5\pi} \quad (24)
\end{aligned}$$

where (21) is based on the Hölder's inequality, the (22) comes from the Minkowski's inequality, and (23) is given by the facts that $|y| \leq 1$ and $|z| \leq 1$. We can also derive an upperbound for the energy, E_2, of $\dot{\vec{v}}_1^T\dot{\vec{p}}_1$ as

$$\begin{aligned}
E_2 &= \int_{-\infty}^{+\infty}\frac{A^4}{L^2}\left(\dot{y}^2 + \dot{z}^2\right)^2 dt \\
&\leq \frac{A^4}{L^2}\left[\sqrt{\int_{-\infty}^{+\infty}\dot{y}^4 dt} + \sqrt{\int_{-\infty}^{+\infty}\dot{z}^4 dt}\right]^2 \quad (25) \\
&\leq \frac{A^4}{L^2}\left(\frac{\sigma W^2}{2\pi}\right)^2\left[\sqrt{\int_{-\infty}^{+\infty}\dot{y}^2 dt} + \sqrt{\int_{-\infty}^{+\infty}\dot{z}^2 dt}\right]^2 \quad (26) \\
&= \frac{A^4}{L^2}\left(\frac{\sigma W^2}{2\pi}\right)^2\left(\sqrt{\frac{\sigma^2 W^3}{3\pi}} + \sqrt{\frac{\sigma^2 W^3}{3\pi}}\right)^2 \\
&= \frac{A^4\sigma^4 W^7}{3L^2\pi^3} \quad (27)
\end{aligned}$$

where (25) comes from the Minkowski's inequality, (26) is based on (20). From (24) and (27), we have

$$\frac{E_2}{E_1} \leq \left(\frac{A}{L}\right)^2 \frac{L}{L-4A} \frac{5\sigma^2 W^2}{3\pi^2} \quad . \tag{28}$$

From similar derivations, we can get upperbounds of energy ratio, which are identical to (28), for all of the struts. For UW's flexure joint hexapod, if we set $W = 160\pi$ rad/sec, and we assume that x, y, and z are uniformly distributed on $(-1, 1)$ (i.e., $\sigma = \frac{1}{3}$), then $\frac{E_2}{E_1} \leq 0.0087$, i.e., the energy of the Coriolis terms is more than two orders of magnitude weaker than that of the acceleration along the strut directions. Note that the orthogonal connection of struts maximizes the generation of Coriolis terms, so these results hold for other flexure jointed hexapods as well. The key is that $\frac{S}{L} \ll 1$. This is true for flexure jointed hexapods. For instance, the Honeywell strut used in MVIS has $\frac{S}{L} = 0.0004$.